PERGAMON

Chemical Engineering Science 58 (2003) 3589–3600

Chemical Engineering Science

www.elsevier.com/locate/ces

Rate-based modelling of SO_2 absorption into aqueous $NaHCO_3/Na_2CO_3$ solutions accompanied by the desorption of CO_2

S. Ebrahimi[a,b,*], C. Picioreanu[a], R. Kleerebezem[a], J. J. Heijnen[a], M. C. M. van Loosdrecht[a]

[a] *Kluyver Laboratory for Biotechnology, Delft University of Technology, Julianalaan 67, 2628 BC Delft, The Netherlands*
[b] *Chemical Engineering Department, Sahand University of Technology, Tabriz, Iran*

Received 21 February 2003; received in revised form 9 May 2003; accepted 16 May 2003

Abstract

A rate-based model of a counter-current reactive absorption/desorption process has been developed for the absorption of SO_2 into $NaHCO_3/Na_2CO_3$ in a packed column. The model adopts the film theory, includes diffusion and reaction processes, and assumes that thermodynamic equilibrium among the reacting species exists in the bulk liquid. Model predictions were compared to experimental data from literature. For the calculation of the absorption rate of SO_2 into $NaHCO_3/Na_2CO_3$ solutions and concomitant CO_2-desorption, it is important to take into account all reversible reactions simultaneously. It is clear that the approximate analytical based model cannot be expected to predict the absorption rates under practical conditions because of the complicated nature of the reactive absorption processes. The rigorous numerical approach described here only requires definition of the individual reactions in the system, and subsequent solution is independent of specific assumptions made, or operational variables like pH or compound concentrations. As an example of the flexibility of this approach, additional calculations were conducted for SO_2 absorption in a phosphate-based buffer system.

Keywords: Absorption; Flue gas; Sulfur dioxide; Numerical analysis; Multiphase reactions; Modelling

1. Introduction

Sulfur dioxide in flue gas generated as a result of combustion of fossil fuel in, e.g., thermal power plants, etc., is the main cause of global environmental problems such as air pollution and acid rain. Sulfur dioxide has also been reported to support the reactions that create ozone depletion in the stratosphere (Karlsson, 1997). Many countries have therefore adopted strict regulations regarding SO_2 emissions from coal- and oil-fired boilers in power plants, which are one of the primary sources of SO_2 emissions. The sulfur dioxide content of the flue gas generated is usually quite small and below about 0.1–0.4% by volume (Astarita, Savage, & Bisio, 1983). However, the volume of the gas produced globally is so large that considerable amount of sulfur dioxide is introduced into the atmosphere. In view of the large number of processes which introduce sulfur dioxide into the atmosphere, it is apparent that studies on flue gas desulfurization methods and development of flue gas desulfurization plants have become numerous.

Although various processes have been proposed for flue gas desulfurization, the wet-type scrubbing is still the dominant process. The wet-type processes include methods using alkaline solutions of sodium, calcium and magnesium compounds as absorbent. The sodium method above all is excellent in reactivity between the absorbent and SO_2, but the sodium compounds used are relatively expensive for this purpose. For this reason, the calcium method using relatively cheap calcium compounds such as calcium carbonate is most widely employed as a flue gas desulfurization system for large boilers in power plants. However, when sodium compounds are used in a closed-loop system (with regeneration of solutions), it is estimated that the costs will be comparable or lower than those of calcium-based processes.

In this study, we have developed a combined chemical/biological process for SO_2 removal, $NaHCO_3$ recovery and elemental sulfur production. An aqueous $NaHCO_3/Na_2CO_3$ solution is used as absorbent in a closed-loop process, schematically depicted in Fig. 1.

* Corresponding author. Kluyver Laboratory for Biotechnology, Delft University of Technology, Julianalaan 67, 2628 BC Delft, The Netherlands. Tel.: +31-15-278-1551; fax: +31-15-278-2355.
E-mail address: s.ebrahimi@tnw.tudelft.nl (S. Ebrahimi).

0009-2509/03/$ - see front matter © 2003 Elsevier Ltd. All rights reserved.
doi:10.1016/S0009-2509(03)00231-8

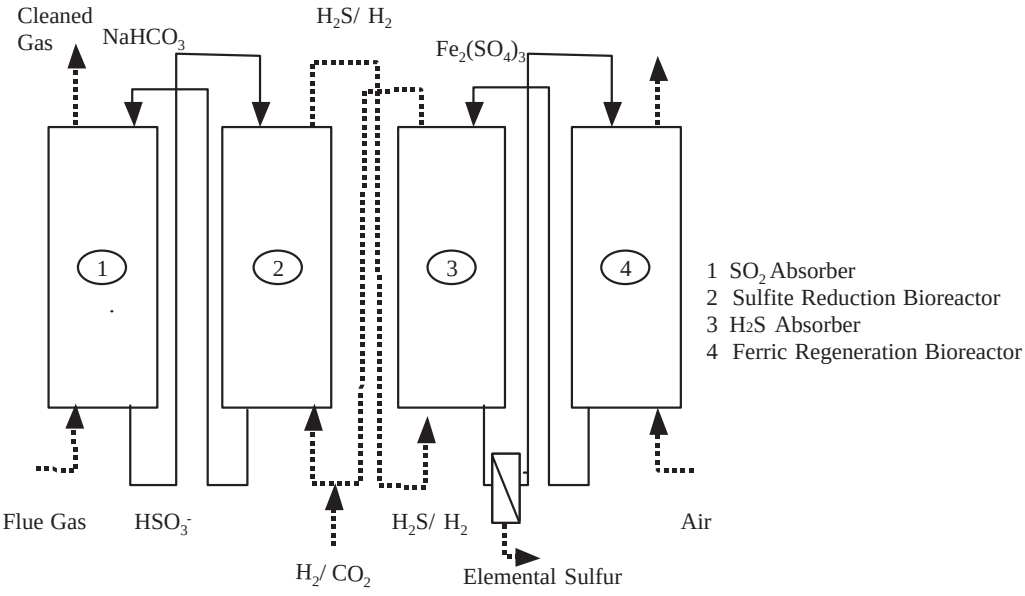

Fig. 1. Process scheme of chemo-biological SO_2 removal.

The process consists of two major liquid circulation loops. The first loop contains a sulfur dioxide absorber, which converts SO_2 into HSO_3^-, and a sulfite reduction bioreactor where HSO_3^- is converted into H_2S, using H_2. In the second loop, an aqueous $Fe_2(SO_4)_3$ solution is used as H_2S absorbent. H_2S is absorbed and oxidized to elemental sulfur, while Fe^{3+} is reduced to Fe^{2+}. Elemental sulfur is removed from the solution by a separator, and the reactant Fe^{3+} is regenerated from Fe^{2+} by biological oxidation in an aerated bioreactor (Ebrahimi, Kleerebezem, van Loosdrecht, & Heijnen, 2003).

The present study aims at developing a rigorous rate-based steady-state model for the design and simulation of packed columns used for absorption of SO_2 into aqueous $NaHCO_3/Na_2CO_3$. The goal is to estimate the absorption rates, enhancement factors and concentration profiles of all chemical species involved. The model is based on the film theory of gas absorption. A numerical solution of the model was used, allowing for integration of the following aspects:

- reversibility effect of all reactions involved;
- the formation, absorption and desorption of CO_2;
- the effect of finite CO_2 reaction rate, and the second dissociation of CO_2;
- the contribution of the gas phase resistance to mass transfer; and
- unequal diffusivities of the species.

There have been a few studies on the mechanism of chemical absorption of SO_2 into aqueous solutions (e.g., Chang & Rochelle, 1981, 1985; Hikita, Asai, & Tsuji, 1977; Hikita & Konishi, 1983; Sada, Kumazawa, & Butt, 1980). In those studies, approximate analytical solutions were used, which limits the applicability to the specific conditions investigated based on simplifying assumptions. Therefore, most of the above-mentioned aspects cannot be studied with the analytical model. As it will be shown later, the use of simplified expressions may easily lead to erroneous results. In this work the expressions for the rate of absorption describing the interfacial fluxes were implemented in design calculations for absorber columns.

2. System description

A gas mixture containing SO_2 is fed at the bottom of the column, schematically shown in Fig. 2, at a volumetric flow rate G. The gas comes in contact with a liquid containing the absorbing reactant flowing from the top at a flow rate L. The following assumptions were made to obtain a mathematical model describing the mass transfer with simultaneous chemical reaction in a differential absorber:

- mass transfer can be described by the film theory;
- isothermal, steady state operation;
- the gas and liquid phases are in plug flow; and
- solute concentrations are low so that the amount of absorption and reactions do not cause a significant change in the flow rates of gas and liquid.

2.1. Chemistry

When dilute sulfur dioxide is absorbed into aqueous $NaHCO_3/Na_2CO_3$ solutions, the following reactions should

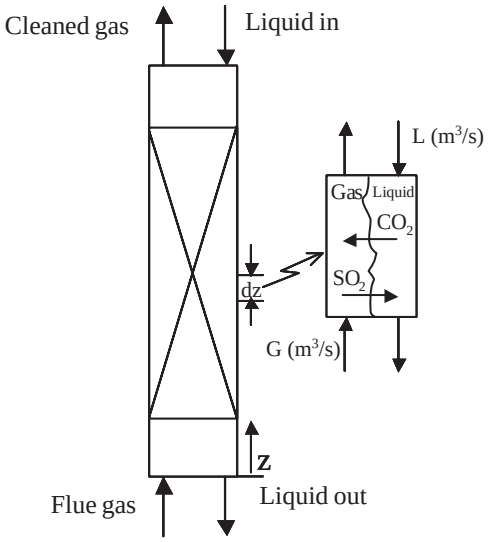

Fig. 2. Countercurrent gas–liquid contacting in packed column.

be considered:

$$SO_2 + H_2O \rightleftarrows H^+ + HSO_3^-, \quad (1)$$

$$HSO_3^- \rightleftarrows H^+ + SO_3^{2-}, \quad (2)$$

$$CO_2 + H_2O \rightleftarrows H^+ + HCO_3^-, \quad (3)$$

$$CO_2 + OH^- \rightleftarrows HCO_3^-, \quad (4)$$

$$HCO_3^- \rightleftarrows H^+ + CO_3^{2-}, \quad (5)$$

$$H_2O \rightleftarrows H^+ + OH^-. \quad (6)$$

Reaction (1) is very fast, with an estimated forward rate constant of 3.4×10^6 (1/s) (Chang & Rochelle, 1981). Reactions (2), (5) and (6) are even faster than reaction (1) since they are based on simple proton transfer and therefore regarded as instantaneous. Consequently, instantaneous equilibrium is assumed for the reactions (1), (2), (5) and (6) throughout the liquid film.

The hydrolysis of CO_2 is slow. Two reactions (3) and (4) may occur when CO_2 is absorbed by aqueous alkaline solutions (Danckwerts, 1970). Forward reaction (3) is pseudo-first order, whereas forward reaction (4) is second order. The rate of reversible reactions (3) and (4) can be expressed as the difference between the forward and the backward reaction rates, respectively:

$$R_{CO_2,1} = k_3(C_{CO_2} - C_{HCO_3^-} C_{H^+}/K_3), \quad (7)$$

$$R_{CO_2,2} = k_4(C_{CO_2} C_{OH^-} - C_{HCO_3^-}/K_4). \quad (8)$$

The rate constant of the forward hydrolysis reactions (3) and (4) can be calculated according to Brogren and Karlsson (1997) and Astarita et al. (1983), respectively:

$$\log(k_3) = 329.85 - 110.541 \log(T) - \frac{17265.4}{T}$$

$$K_3(1/s) \text{ and } T(K) \quad (9)$$

$$\log(k_4) = 13.635 - 2895/T + 0.08I$$

$$K_4(m^3/Kmol \cdot s) \text{ and } T(K). \quad (10)$$

In any solution of pH $\geqslant$ 10, the CO_2 reaction rate according to Eq. (4) will be more than 30 times higher than that consumed in reaction (3). Thus, reaction (3) is normally of negligible importance in determining the rate of absorption of CO_2 into alkaline solutions with pH $\geqslant$ 10. However, at pH values below 8, as in our process, reaction (3) is faster than reaction (4) (Astarita et al., 1983; Danckwerts, 1970).

In this model the sulfite oxidation reaction has not taken into account because of the relatively low reaction rate (Eden & Luckas, 1998).

2.2. Reactor model

The steady-state mass balance for SO_2 and CO_2 in the gas phase plug flow through the column can be written as

$$\left(\frac{G}{RTS}\right)\frac{dp_{SO_2,b}}{dz} = -N^g_{SO_2,i}a, \quad (11)$$

$$\left(\frac{G}{RTS}\right)\frac{dp_{CO_2,b}}{dz} = -N^g_{CO_2,i}a. \quad (12)$$

The steady-state mass balance for each species (A) in the bulk liquid phase, also assumed in plug flow, is

$$\frac{L}{S}\frac{dC_{A,b}}{dz} = N^l_{A,b}a + R^l_{A,b}\varepsilon_l. \quad (13)$$

The mass balances for individual species can be combined to obtain mass balances for total S and C species. Furthermore, according to the law of elemental conservation, the steady-state fluxes of total S and C species through the liquid film are constant and are equal to SO_2 and CO_2 fluxes at the gas side ($N^l_{S\_total,b} = N^g_{SO_2,i}$ and $N^l_{C\_total,b} = N^g_{CO_2,i}$). Therefore, a continuity equation for total S and C species in the liquid phase can be written as

$$\frac{L}{S}\frac{dC_{S\_total,b}}{dz} = N^g_{SO_2,i}a, \quad (14)$$

$$\frac{L}{S}\frac{dC_{C\_total,b}}{dz} = N^g_{CO_2,i}a. \quad (15)$$

Eqs. (11), (12), (14) and (15) contain the fluxes $N^g_{SO_2,i}$ and $N^g_{CO_2,i}$. These fluxes are related to the concentration gradients of SO_2 and CO_2 at the gas/liquid interface (see Eqs. (27) and (29)), so that the concentration profiles of SO_2 and CO_2 in the liquid film are required. For this purpose, the mass balance equations in liquid film for different species have to be integrated.

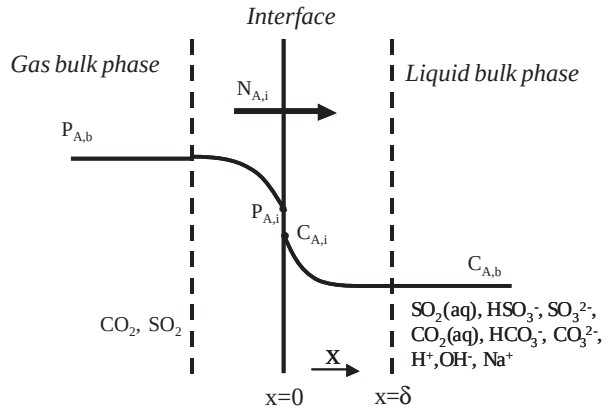

Fig. 3. Schematic diagram of the two film model.

2.3. Film region

The mass transfer between the gas and liquid phase is described based on the film model. Even though film renewal theory for gas liquid mass transfer represents the most realistic mass transfer model conditions, it is rarely used in practice since this leads to a complex mathematical description and evaluation of reacting systems. In the film model, all the resistance to mass transfer is concentrated in a thin film adjacent to the phase interface and the mass transfer occurs within this film by steady-state molecular diffusion (Kenig, Schneider, & Górak, 1999) (Fig. 3). Reactions between the absorbed gas and the liquid reactants are assumed to be complete within the liquid film. This implies that the bulk liquid is in a state of chemical equilibrium.

Since the chemical reactions occur only in the liquid phase, the molar flux of each component in the gas-phase film is constant along the direction x (i.e., normal to the gas/liquid interface). The differential equations describing the diffusion of each component A in the gas phase (without reaction) have the following form:

$$\frac{dN_A^g}{dx} = 0.$$

The differential equations describing the process of diffusion with simultaneously reaction of each species A in the liquid phase are

$$\frac{dN_A^l}{dx} = R_A. \tag{16}$$

The simple Fick's law is used to express the diffusive flux of each species:

$$N_A = -D_A \frac{dC_A}{dx}. \tag{17}$$

After replacing the fluxes (17) in Eqs. (16), the mass balances for individual species can be combined to obtain the following balances for total sulfite, total carbonate and total sodium:

$$D_{SO_2} \frac{d^2C_{SO_2}}{dx^2} + D_{HSO_3^-} \frac{d^2C_{HSO_3^-}}{dx^2} + D_{SO_3^{2-}} \frac{d^2C_{SO_3^{2-}}}{dx^2} = 0, \tag{18}$$

$$D_{CO_2} \frac{d^2C_{CO_2}}{dx^2} + D_{HCO_3^-} \frac{d^2C_{HCO_3^-}}{dx^2} + D_{CO_3^{2-}} \frac{d^2C_{CO_3^{2-}}}{dx^2} = 0, \tag{19}$$

$$D_{Na^+} \frac{d^2C_{Na^+}}{dx^2} = 0. \tag{20}$$

Because the hydrolysis reaction of CO_2 is slow, a separate material balance for CO_2 has to be included:

$$D_{CO_2} \frac{d^2C_{CO_2}}{dx^2} - R_{CO_2,1} - R_{CO_2,2} = 0. \tag{21}$$

It has been shown that the impact of any electric potential gradient on the flux of ions may be disregarded under flue gas desulfurization conditions as long as the mass flux equations are combined with a flux charge equation (Brogren & Karlsson, 1997). Therefore, the mass balances must be combined with a flux of charge balance when the potential gradient is disregarded. The flux of charge in the liquid film:

$$\begin{aligned} &D_{H^+} \frac{dC_{H^+}}{dx} + D_{Na^+} \frac{dC_{Na^+}}{dx} - D_{OH^-} \frac{dC_{OH^-}}{dx} \\ &- D_{HSO_3^-} \frac{dC_{HSO_3^-}}{dx} - 2D_{SO_3^{2-}} \frac{dC_{SO_3^{2-}}}{dx} \\ &- D_{HCO_3^-} \frac{dC_{HCO_3^-}}{dx} - 2D_{CO_3^{2-}} \frac{dC_{CO_3^{2-}}}{dx} = 0. \end{aligned} \tag{22}$$

Since instantaneous equilibrium is assumed for the reactions (1), (2), (5) and (6) throughout the liquid film, the chemical equilibrium relations of these reactions also apply at all points in liquid phase:

$$\frac{C_{H^+}C_{HSO_3^-}}{C_{SO_2}} = K_1, \tag{23}$$

$$\frac{C_{H^+}C_{SO_3^{2-}}}{C_{HSO_3^-}} = K_2, \tag{24}$$

$$\frac{C_{H^+}C_{CO_3^{2-}}}{C_{HCO_3^-}} = K_5, \tag{25}$$

$$C_{H^+}C_{OH^-} = K_6. \tag{26}$$

2.4. Boundary conditions

The model system consisting of mass and charge balances Eqs. (18)–(22) and the chemical equilibrium relations (23)–(26) must be completed by the boundary conditions relevant to the film model at $x = 0$ and δ.

2.4.1. Boundary conditions at the interface ($x = 0$)

The absorption rate of SO_2 is equal to the sum of the fluxes of the sulfur species at the gas–liquid interface, which also must be equal to the flux of SO_2 in the gas film:

$$N^g_{SO_2,i} = \frac{k_{g,SO_2}}{RT}\,(p_{SO_2,b} - p_{SO_2,i}) = -\left(D_{SO_2}\left.\frac{dC_{SO_2}}{dx}\right|_{x=0} + D_{HSO_3^-}\left.\frac{dC_{HSO_3^-}}{dx}\right|_{x=0} + D_{SO_3^{2-}}\left.\frac{dC_{SO_3^{2-}}}{dx}\right|_{x=0}\right), \quad (27)$$

where

$$p_{SO_2,i} = H_{SO_2} C_{SO_2,i}. \quad (28)$$

Since the rate of the hydrolysis reaction is slow, the flux of CO_2 in the gas film is equal to the flux of dissolved CO_2 at the interface:

$$N^g_{CO_2,i} = k_{g,CO_2}/RT(p_{CO_2,b} - p_{CO_2,i}) = -D_{CO_2}\left.\frac{dC_{CO_2}}{dx}\right|_{x=0}, \quad (29)$$

where

$$p_{CO_2,i} = H_{CO_2} C_{CO_2,i}. \quad (30)$$

The flux of HCO_3^- and CO_3^{2-} at the interface must be zero because the transport of carbon species is represented by CO_2:

$$D_{HCO_3^-}\left.\frac{dC_{HCO_3^-}}{dx}\right|_{x=0} + D_{CO_3^{2-}}\left.\frac{dC_{CO_3^{2-}}}{dx}\right|_{x=0} = 0. \quad (31)$$

The flux of Na is zero at the interface:

$$D_{Na^+}\left.\frac{dC_{Na^+}}{dx}\right|_{x=0} = 0 \quad (32)$$

and also the net flux of charge must be zero at $x = 0$:

$$D_{H^+}\left.\frac{dC_{H^+}}{dx}\right|_{x=0} + D_{Na^+}\left.\frac{dC_{Na^+}}{dx}\right|_{x=0} - D_{OH^-}\left.\frac{dC_{OH^-}}{dx}\right|_{x=0} - D_{HSO_3^-}\left.\frac{dC_{HSO_3^-}}{dx}\right|_{x=0} - 2D_{SO_3^{2-}}\left.\frac{dC_{SO_3^{2-}}}{dx}\right|_{x=0} - D_{HCO_3^-}\left.\frac{dC_{HCO_3^-}}{dx}\right|_{x=0} - 2D_{CO_3^{2-}}\left.\frac{dC_{CO_3^{2-}}}{dx}\right|_{x=0} = 0. \quad (33)$$

Instantaneous equilibrium is assumed for the reactions (1), (2), (5) and (6) at the interface, thus Eqs. (23)–(26) apply also at $x = 0$.

2.4.2. Boundary conditions in bulk liquid ($x = \delta$)

Equilibrium is assumed for the all reactions in the bulk liquid, therefore, besides mass action laws (23)–(26) also equilibrium equation:

$$\frac{C_{H^+} C_{HCO_3^-}}{C_{CO_2}} = K_3, \quad (34)$$

is considered, together with another four equations obtained from mass balances for total sulfur species, total carbon species, sodium and a charge balance:

$$C_{tot,S} = C_{SO_2,b} + C_{HSO_3^-,b} + C_{SO_3^{2-},b}, \quad (35)$$

$$C_{tot,C} = C_{CO_2,b} + C_{HCO_3^-,b} + C_{CO_3^{2-},b}, \quad (36)$$

$$C_{tot,Na} = C_{Na^+,b}, \quad (37)$$

$$C_{H^+} + C_{Na^+} - C_{OH^-} - C_{HSO_3^-} - 2C_{SO_3^{2-}} - C_{HCO_3^-} - 2C_{CO_3^{2-}} = 0. \quad (38)$$

The system of equations (18)–(22) together with the four equilibrium equations (23)–(26) and the boundary conditions (27)–(38) are used to find the concentration profiles of the nine unknown species in the liquid film ($SO_2, HSO_3^-, SO_3^{2-}, CO_2, HCO_3^-, CO_3^{2-}, Na^+, H^+, OH^-$) at each position z in the column height. These concentration profiles allow the calculation of the fluxes of SO_2 and CO_2. The fluxes are needed for integration of differential mass balance equations in the bulk gas and liquid along the column (11), (12), (14) and (15).

The liquid film thickness and reactor height were both discretized in a spatially uniform grid and second-order finite differencing was applied. The resulting system of non-linear algebraic equations was solved numerically with a traditional Newton-based method.

3. Estimation of physical properties and model parameters

The diffusion coefficients of gases were calculated from the equation given by Reid, Prausnitz, and Poling (1988). The diffusion coefficients in liquid, used in model calculations, are listed in Table 1. The diffusion constants were extrapolated from 25°C to 55°C using the Stokes–Einstein equation:

$$\frac{D_A \mu}{T} = \text{constant}. \quad (39)$$

Correlations for the determination of the dissociation equilibrium constants and solubility values for SO_2 and CO_2 as a function of temperature are given in Table 2. The activity coefficients γ take into account the deviations of the thermodynamic equilibrium of real mixture from those of an ideally diluted solution. Depending on whether species are charged or not, two different types of activity coefficient

Table 1
Effective diffusitivities in water at 25°C and infinite dilution, D_A (Vanysek, 2001)

Species	D_A (m^2/s)
H^+	9.311×10^{-9}
Na^+	1.334×10^{-9}
OH^-	5.273×10^{-9}
SO_2(aq)	1.83×10^{-9}
HSO_3^-	1.545×10^{-9}
SO_3^{2-}	0.959×10^{-9}
CO_2(aq)	1.91×10^{-9}
HCO_3^-	1.185×10^{-9}
CO_3^{2-}	0.923×10^{-9}

expressions are:

- Simple salting relation for uncharged species A (Gerard, Segantini, & Vanderschuren, 1996; Hikita et al., 1977)

$$\log \gamma_A = 0.076I. \tag{40}$$

- Extended Debye–Hückel model (B dot equation) for individual ions (Parkhurst & Appelo, 1999)

$$\log \gamma_A = -\frac{Az_A^2\sqrt{I}}{1 + Ba_A\sqrt{I}} + \dot{B}I. \tag{41}$$

The following correlations, which cover a wide range of packing types, sizes and test systems, were used to calculate individual mass transfer coefficients (k_l and k_g) and the interfacial area (a) for packed column (Onda, Sada, & Okumoto, 1968a; Onda, Takahashi, & Okumoto, 1968b):

$$k_g(RT/a_pD_g) = 5.23(G'/a_p\mu_g)^{0.7}(\mu_g/\rho_gD_g)^{1/3} \times (a_pd_p)^{-2}, \tag{42}$$

$$k_l(\rho_l/g\mu_l) = 0.0051(L'/a\mu_l)^{2/3}(\mu_l/\rho_lD_l)^{-0.5} \times (a_pd_p)^{0.4}, \tag{43}$$

$$a = a_p(1 - \exp[-1.45(L'/a\mu_l)^{0.1}(a_pL'^2/g\rho_l^2)^{-0.05} \times (L'^2/a_p\sigma\rho_l)^{0.2}(\sigma/\sigma_c)^{-0.75}]). \tag{44}$$

The mass transfer coefficient k_l was used for the estimation of the thickness of mass transfer boundary layer in the liquid phase, δ, using the diffusivity for SO_2 as reference: $\delta = D_{SO_2}/k_{l,SO_2}$.

4. Results and discussion

4.1. Model validation

Validation of the developed film model was established using SO_2 absorption data into aqueous Na_2CO_3 solutions as presented by Hikita and Konishi (1983).

These authors have carried out absorption experiments using a baffled agitated vessel operated batchwise with respect to the liquid, and compared the experimental results with an approximate analytical solution based on the Leveque model. They proposed a two reaction plane model and showed that the measured absorption and desorption rates were in good agreement with the theoretical predictions.

Using the same parameters and conditions as used by Hikita and Konishi (1983), the pH and concentration profiles for all species were calculated and the results are shown in Fig. 4. These concentration profiles clearly show the rapid depletion of SO_2 near the gas–liquid interface and agree with the existence of the two reaction planes in this system. These two reaction planes divide the liquid phase into three regions. Therefore, the intuitive profiles suggested by Hikita and Konishi (1983) for similar cases agree well with the more exact prediction of our model.

As suggested by Hikita and Konishi (1983) the following four reactions may occur irreversibly and instantaneously at

Table 2
Effect of temperature on dissociation constants of weak electrolytes in water, K, and solubility coefficients of gases in pure water, H

Reaction	A	B	C	D	Range of validity, °C	Ref.
$\ln(K) = A/T + B\ln(T) + C(T) + D$ $K(mol/kg)$ and $T(K)$						
$CO_2 + H_2O \rightleftarrows HCO_3^- + H^+$	−12092.1	−36.7816	0	235.482	0–225	a
$HCO_3^- \rightleftarrows H^+ + CO_3^{2-}$	−12431.7	−35.4819	0	220.067	0–225	a
$SO_2 + H_2O \rightleftarrows HSO_3^- + H^+$	26404.29	160.3981	−0.275224	−924.6255	–-	b
$HSO_3^- \rightleftarrows H^+ + SO_3^{2-}$	−5421.93	−4.6899	−0.0498769	43.3136	–-	b
$H_2O \rightleftarrows OH^- + H^+$	−13445.9	−22.4773	0	140.932	0–225	a
$\ln(H) = A/T + B\ln(T) + C(T) + D$ $H(atm.kg/mol)$ and $T(K)$						
CO_2	−6789.04	−11.4519	−0.010454	94.4914	0–250	a
SO_2	−5578.8	−8.76152	0	68.418	0–100	a

(a) Edward, Maurer, and Prausnitz (1978); (b) Xia, Rumpf, and Maurer (1999).

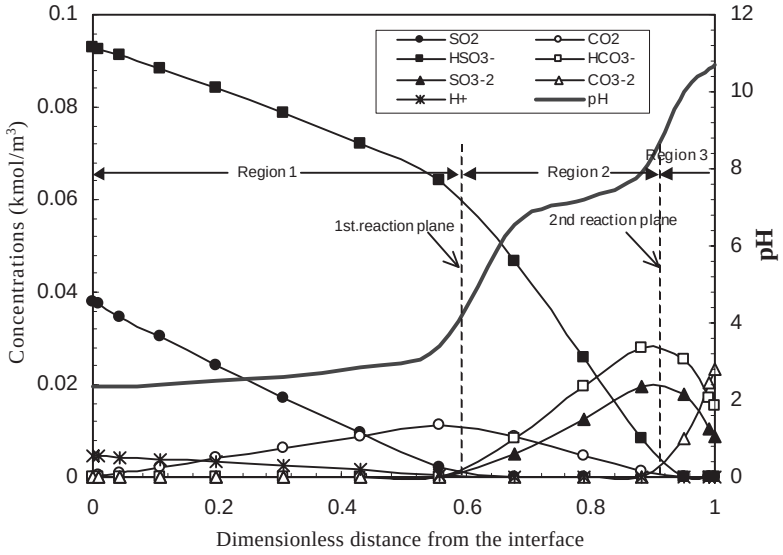

Fig. 4. Concentration profiles calculated for the absorption of SO_2 into aqueous Na_2CO_3 solution in the liquid film. Na_2CO_3: 0.0398 kmol/m^3; $SO_{2,i}$: 0.0379 kmol/m^3 and $CO_{2,i}$: 0.0000603 kmol/m^3; $\delta = 0.00013$ m.

the first reaction plane:

$$SO_2 + SO_3^{2-} + H_2O \rightarrow 2HSO_3^-, \quad (45)$$

$$SO_2 + HCO_3^- \rightarrow CO_2 + HSO_3^-, \quad (46)$$

$$H^+ + HCO_3^- \rightarrow CO_2 + H_2O, \quad (47)$$

$$H^+ + SO_3^{2-} \rightarrow HSO_3^-. \quad (48)$$

At the second reaction plane, the following instantaneous irreversible reaction take place:

$$CO_3^{2-} + HSO_3^- \rightarrow SO_3^{2-} + HCO_3^-. \quad (49)$$

In addition, the hydrolysis reaction of SO_2 may occur instantaneously and reversibly in region 1. Because in regions 2 and 3, CO_2 and SO_3^{2-} ions coexist, these two species can react according to

$$CO_2 + SO_3^{2-} + H_2O \rightleftarrows HSO_3^- + HCO_3^-. \quad (50)$$

Some of the CO_2 liberated at the first reaction plane diffuses towards the bulk of the liquid. The remainder of CO_2 diffuses towards the gas–liquid interface and desorbs into the gas phase if the concentration of CO_2 at the first reaction plane is greater that at the interface.

The predictions of the proposed analytical model by Hikita and Konishi (1983) and our theoretical model for the absorption and desorption rates for SO_2 and CO_2 against the experimental results are shown in Figs. 5a and b respectively. It can be seen that the theoretical rates computed with both models are in good agreement with the measured absorption and desorption rates in Na_2CO_3 solutions.

The proposed analytical model by Hikita and Konishi (1983) is in good agreement with the experimental data in this particular case. However, the analytical model cannot be expected to predict the absorption/desorption rates for a wide range of conditions. At high concentration of Na_2CO_3, for example, the two reaction plane model is not realistic because the assumption of zero concentrations for specific reactants will not hold. Moreover, the model presented in this study gives a more general solution for chemical absorption of SO_2 at different concentration of aqueous alkaline solution (NaOH and $NaHCO_3/Na_2CO_3$) and various SO_2 and CO_2 partial pressures in the gas phase. In addition, the pH profile is directly calculated in the liquid film.

4.2. Scrubber design

The proposed model is applied to the design of a scrubber for the removal of SO_2 from the flue gas in a power plant. In the present example, flue gas from a 600 MW power plant containing 1000 ppm SO_2 (0.1 vol%) is to be purified by absorption into an aqueous $NaHCO_3/Na_2CO_3$ solution. The inlet flow rate of gas is 2×10^6 Nm^3/h. The temperature is 110°C and the total pressure is 1.1 bar. The partial pressure of CO_2 in the flue gas amounts 0.14 bar.

If incoming gas streams are at elevated temperatures, the first function of the scrubber normally is to saturate the gas with water and cool the gas. Usually the cooling is adiabatic, that is, the gas is saturated by the scrubbing liquid until the temperatures of the water and the gas are the same. The objective of this preliminary step, which may be achieved in an early stage of the scrubber or in a preliminary saturation chamber, is to reduce the volume of gas entering the subsequent stages of the scrubber. Hence, the preliminary step reduces the equipment size and lower the total capital cost. Herewith, evaporation can be prevented in subsequent

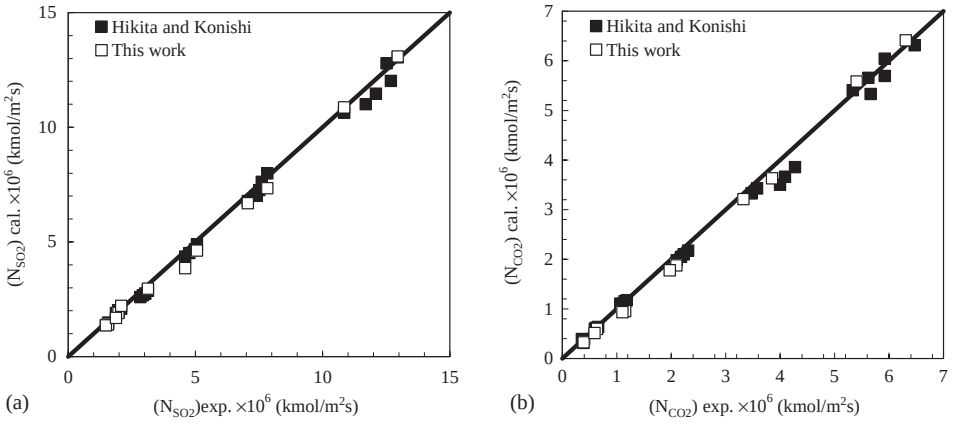

Fig. 5. SO_2 absorption into aqueous Na_2CO_3 solutions. Comparison between theoretical absorption/desorption rates and experimental data from Hikita and Konishi (1983). Na_2CO_3 = 39.8– 994 mol/m^2; $SO_{2,i}$ = 22.5–48.9 mol/m^3; $CO_{2,i}$ = 0.0548–0.376 mol/m^3. (a) SO_2 absorption rate; (b) CO_2 desorption rate.

stages where loss of water vapour might cause precipitation of unwanted compounds on scrubber surfaces, and subsequent stages of the scrubber are protected from the potentially corrosive effects of heated gas (McCarthy, 1980). For these reasons, design calculations were made for saturated flue gas at a temperature of 55°C.

The desulfurization methods using sodium compounds in the absorbent liquid can be generally classified into spraying, wetted-wall and bubbling systems, depending on the particular gas–liquid contacting method. Since the packed and spray column systems are considerably more popular and reliable, here the results of model calculations for a packed column are presented.

The liquid phase enters the column at the top and flows in countercurrent with the gas. The height of the column is determined for 95% removal of SO_2 from the flue gas when 0.05 kmol/m^3 bicarbonate solution is used as absorbent. The choice of the packed column diameter is based on the 60% of flooding condition. The packed column calculation was based on using a relatively high capacity packing material (35 mm Pal rings). In practice, the gas flow rate should be split and a few smaller columns would operate in parallel. The calculated results are summarized in Table 3.

Table 3
Design parameters and design results for the SO_2 absorption column

T (K)	328
P (bar)	1.1
Flow rates	
G (m^3/s)	556
L (m^3/s)	1.11
Inlet gas phase composition	
p_{SO_2} (bar)	0.0011
p_{CO_2} (bar)	0.14
Inlet liquid phase composition	
C_{NaHCO_3} (kmol/m^3)	0.05
Mass transfer coefficients	
k_{G,SO_2} (m/s)	0.036
k_{G,CO_2} (m/s)	0.0402
k_{L,SO_2} (m/s)	0.0002852
k_{L,CO_2} (m/s)	0.000303
Interfacial area	
a (m^2/m^3)	84.1
% of flooding	60
Calculated column height (m)	2.09
Calculated column diameter (m)	19.1

4.2.1. Concentration profiles in the liquid film

The typical calculated pH and concentration profiles for the various chemical species in the liquid film in the packed column are shown in Fig. 6. SO_2 depletion close to the gas–liquid interface corresponds to the very fast reactions, causing a high enhancement of SO_2 transfer. It is apparent that a large pH drop occurs close to the gas–liquid interface due to SO_2 absorption. One reaction plane can be recognized via the concentration profiles in the liquid film. The reaction plane is located at $x = \lambda$, and it divides the liquid film into two regions. The first region is near the interface, where concentration of SO_2 is significant, and the second one is near the bulk liquid where concentration of SO_2 is negligible. It seems that the substantial reactions take place only at this reaction plane. The most important reaction in first region is the hydrolysis reaction of SO_2, which occurs instantaneously and reversibly.

4.2.2. Partial pressure and mass transfer rates along the column

The partial pressure profiles of SO_2 and CO_2 in the gas bulk along the column are shown in Fig. 7. As the gas moves up the column the partial pressure of SO_2 decreases due to absorption. At the top of the column the partial pressure of

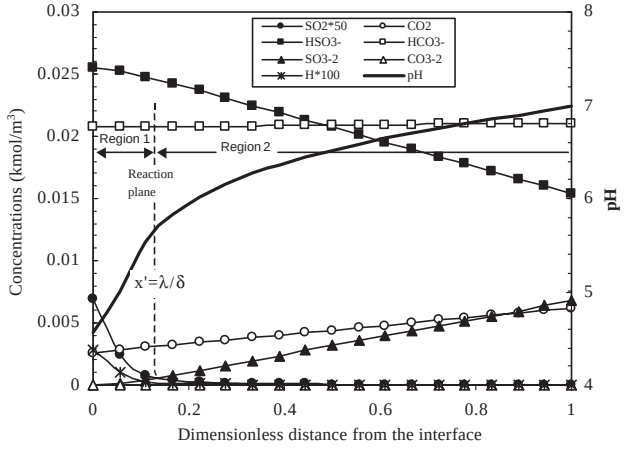

Fig. 6. Absorption of SO_2 and CO_2 in 0.05 M $NaHCO_3$ solution in a packed column. Concentration profiles in the liquid film at $z = 0$ m, $\delta = 1.2 \times 10^{-5}$. Concentrations of SO_2 and H^+ shown in the graph were multiplied by a factor of 50 and 100 respectively.

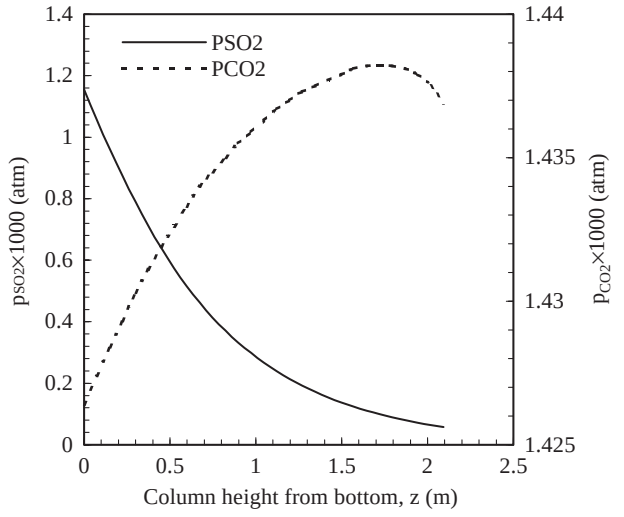

Fig. 7. Partial pressure of SO_2 and CO_2 in the flue gas along the column ($NaHCO_3 = 0.05$; $L/G = 2 \times 10^{-3}$).

CO_2 is higher than the initial backpressure from the aqueous solution. Hence, CO_2 is absorbed in the fresh alkaline solution at the column top. As the pH decreases from the top to the bottom due to the SO_2 absorption, the concentration of CO_2 in the liquid increases and the direction of the CO_2 flux at the gas/liquid interface is reversed because the concentration of CO_2 in the liquid bulk becomes larger than at the interface. CO_2 desorption also occurs when the concentration in the reaction plane is larger than that at the interface, even if in the bulk it may be lower. This CO_2 concentration peak makes therefore possible the apparition of opposed directions of CO_2 diffusion in the liquid film.

The presence of both absorption and desorption in the column is further illustrated by the interfacial mass transfer rates of SO_2 and CO_2 along the column, shown in Fig. 8.

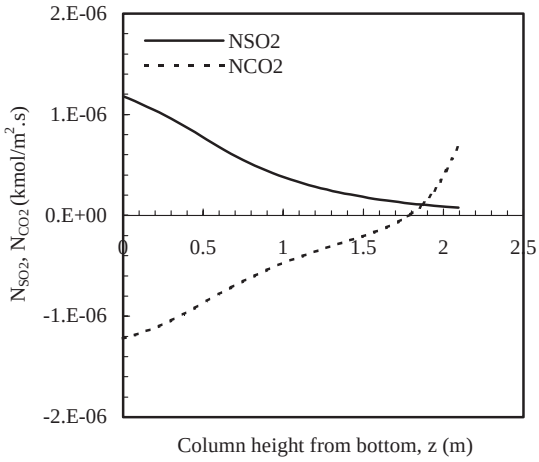

Fig. 8. Mass transfer rate of SO_2 and CO_2 in the flue gas along the column ($NaHCO_3 = 0.05$; $L/G = 2 \times 10^{-3}$).

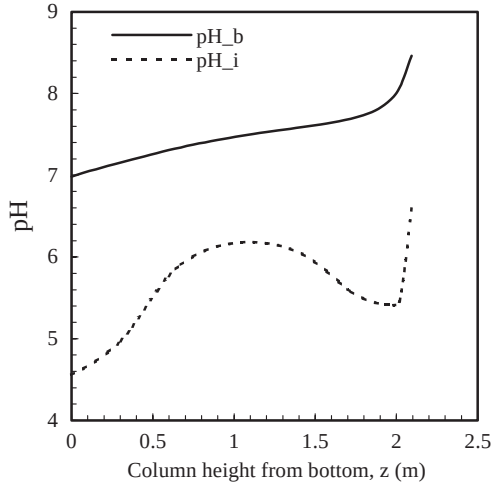

Fig. 9. pH profiles in the liquid bulk and interface along the column ($NaHCO_3 = 0.05$; $L/G = 2 \times 10^{-3}$).

Positive values of the component flux correspond to absorption, whereas negative values represent desorption.

4.2.3. pH profiles along the column

In Fig. 9, the pH profile in the liquid bulk and at the interface along the column is shown. Since the absorption of SO_2 into aqueous $NaHCO_3$ solutions is accompanied by the desorption of CO_2, there is no strong change in pH of the bulk liquid (only 1.5 units of pH). A steep and flux dependent pH-gradient in the liquid film layer is the result from the complex absorption of SO_2 and absorption–desorption behaviour of CO_2.

4.2.4. Enhancement factor and individual film resistances

The model results enable us to evaluate the enhancement factor for chemical absorption at assigned gas and liquid bulk compositions. The enhancement factor, E,

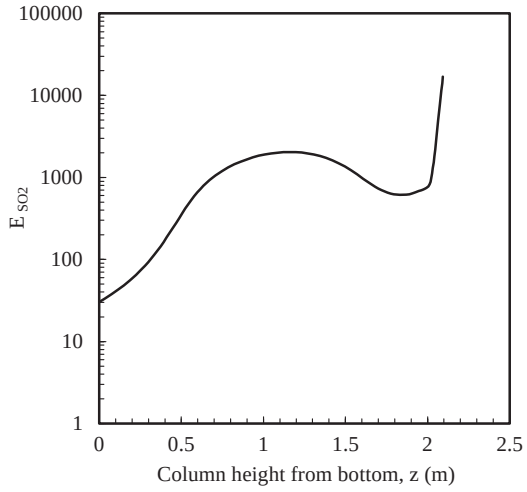

Fig. 10. Chemical enhancement factor for SO_2 absorption along the column ($NaHCO_3 = 0.05$; $L/G = 2 \times 10^{-3}$).

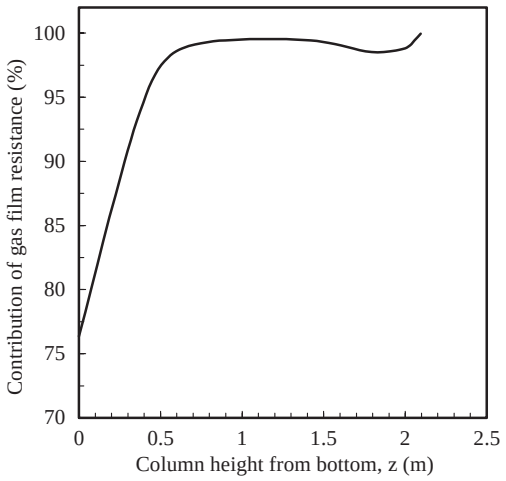

Fig. 11. Contribution of the gas film resistance for SO_2 transfer along the column ($NaHCO_3 = 0.05$; $L/G = 2 \times 10^{-3}$).

considers the effect of the chemical reactions on the liquid-side mass transfer, and is defined as the ratio between the actual absorption rate and the rate that would be observed with the same driving force in the absence of chemical reactions:

$$E = \frac{N_{SO_2}}{(D_{SO_2(aq)}/\delta)(C_{SO_2(aq)}|_{x=0} - C_{SO_2(aq)}|_{x=\delta})}. \quad (51)$$

The enhancement factor for SO_2 absorption (Fig. 10) has its highest value in the top of the absorber, where the partial pressure of SO_2 is low and the alkalinity of the liquid is high. The enhancement factor decreases towards the bottom of the column due to the pH drop. However, a major part of the scrubber operates at a high enhancement factor. That means the absorption is strongly enhanced by the very fast reactions and therefore the gas side resistance to mass transfer becomes important.

At the top of the absorber the contribution of the relative gas film resistance has its largest value as illustrated in Fig. 11. In the condition used in these calculations, the contribution of the gas film resistance is about 100% and 75% in the top and bottom of the absorber respectively. The calculations show that the absorption of SO_2 within a packed scrubber to a large extent is gas side controlled.

4.2.5. Effect of buffer concentration

In Fig. 12 the effect of the sodium bicarbonate concentration on the calculated height of the column is shown. It is apparent that sodium bicarbonate solution above 0.05 kmol/m^3 has enough buffer capacity for SO_2 absorbed, and therefore, a higher concentration of sodium bicarbonate does not have a significant effect on the mass transfer coefficient of either SO_2 or CO_2. Therefore, there is no substantial change in the calculated column height when bicarbonate concentrations higher than 0.05 kmol/m^3 are applied. This invariance of the necessary column height

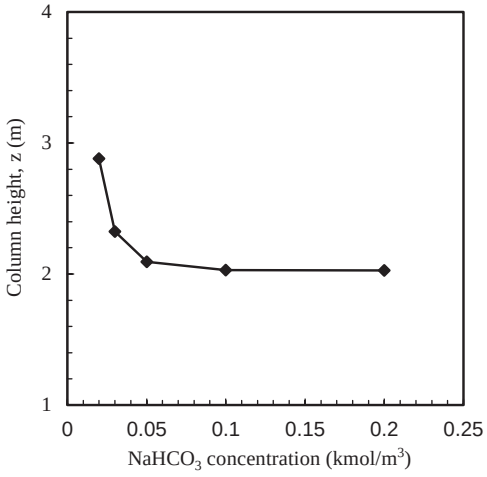

Fig. 12. Dependency of the design column height on the bicarbonate concentration in the inlet liquid ($NaHCO_3 = 0.05$; $L/G = 2 \times 10^{-3}$).

is due to the fact that the mass transfer rate for CO_2 is not affected by chemical reaction and transfer of SO_2 is controlled by gas-side resistance. Consequently, the rate of SO_2 removal can be best improved by creating more turbulence in the gas-phase and thereby higher gas phase mass transport coefficients and by increasing the surface area available for mass transfer.

In the proposed process for SO_2 removal, aqueous absorbent solution from the scrubber is regenerated in a sulfite reduction bioreactor (see Fig. 1). From a biological point of view, pH variation of the aqueous solution should be limited. Increasing buffer capacity of the aqueous solution can decrease the pH drop along the column height. Even though by using higher concentrations of the bicarbonate solution buffer capacity can be increased, on the other hand pH in the column will be increased (see Fig. 13), which is unfavourable for microorganisms. Therefore, it

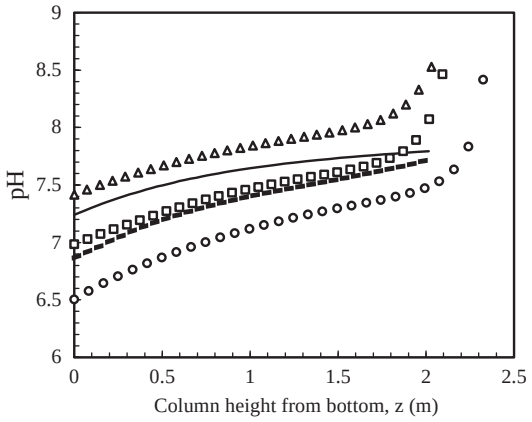

Fig. 13. pH profile in the liquid bulk along the absorber column; the effect of using different buffers ($NaHCO_3 = 0.05$; $L/G = 2 \times 10^{-3}$). (△)$NaHCO_3 = 0.1$ M; (□) $NaHCO_3 = 0.05$ M; (○) $NaHCO_3 = 0.03$ M; (—) $NaHCO_3 = 0.05$ M, $Na_2HPO_4 = 0.025$ M and $NaH_2PO_4 = 0.025$ M; (- - -) $NaHCO_3 = 0.03$ M, $Na_3HPO_4 = 0.015$ M and $NaH_2PO_4 = 0.015$ M.

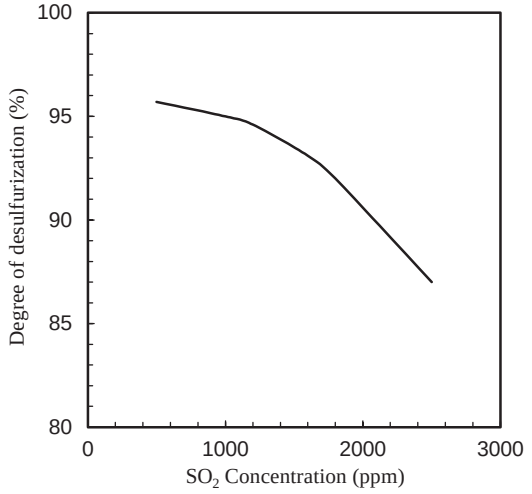

Fig. 14. The effect of the flue gas SO_2 concentration on the column performance ($NaHCO_3 = 0.05$ M; $L/G = 2 \times 10^{-3}$; $H = 2.09$ m).

is interesting to study the effect of a non-volatile buffer solution like phosphate buffer. The numerical model enables us to predict the absorption/desorption rates in such a complex system. In Fig. 13 the effect of two bicarbonate and phosphate buffer on the bulk pH profiles along the column is shown. It is apparent from Fig. 13 that by using phosphate buffer not only buffer capacity can be increased but also the pH in the column can be maintained in the proper range.

4.2.6. *Effect of* SO_2 *gas concentration*

In power plants the SO_2 content of the generated flue gas may vary strongly depending on the type of coal being burned. The effect of different SO_2 concentrations was evaluated and the results are shown in Fig. 14. By increasing the concentration of SO_2 in the flue gas from 1000 to 2000 ppm, the degree of the desulfurization decrease from 95% to 89.5%. Therefore, it can be concluded that the degree of desulfurization is not very sensitive to SO_2 content of the flue gas.

5. Conclusion

In this study, a general approach to the modelling and design of multicomponent reactive absorption/desorption is presented. The complicated absorption process of SO_2 into aqueous $NaHCO_3$/ Na_2CO_3 solutions accompanied by the desorption of CO_2 is well described by the proposed model. The model developed, in spite of simple description of the mass transfer, is capable of accurate prediction of the transfer rates of absorption/desorption and of the enhancement factors. Moreover, the model could predict the concentrations of all chemical species at any point of the absorption column. The model is validated using a SO_2 absorption process in aqueous Na_2CO_3 solutions. The model presented can be applied to any highly complicated reactive absorption/desorption processes. It should be stressed that analytical approximations are often oversimplified and cannot be expected to predict the absorption/desorption rates for a wide range of conditions and so under practical conditions.

Notation

a	wetted surface area of packing, m^2/m^3
a_p	total surface area of packing, m^2/m^3
C	molar concentration in the liquid phase, $kmol/m^3$
$C^l_{A,b}$	concentration of the component A in the liquid bulk, $kmol/m^3$
d_p	diameter of packing, m
D	diffusion coefficient, m^2/s
E_A	enhancement factor
g	gravitational constant, m/s^2
G	gas volume flow rate, m^3/s
G'	gas superficial mass velocity, kg/m^2s
He	Henry's law coefficient, atm $m^3/kmol$
I	ionic strength, $kmol/m^3$
k	reaction rate constant
k_g	gas side mass transfer coefficient, m/s
k_l	liquid side mass transfer coefficient, m/s
L	liquid volume flow rate, m^3/s
L'	liquid superficial mass velocity, kg/m^2 s
N	flux of component A per unit gas–liquid interfacial area, $kmol/m^2$ s
$N^g_{A,i}$	interfacial flux of component A per unit gas–liquid interfacial area, $kmol/m^2$ s
p_A	partial pressure of the component A, atm
P	total pressure, atm
R	gas constant, m^3 atm/kmol K

R_A reaction rate of the component A, kmol/m^3 s
S column cross-section, m^2
T temperature, K
x spatial coordinate in the liquid film, m
z spatial coordinate on the column height, m
z_A electric charge of species A

Greek letters

δ liquid film thickness, m
ε_l liquid hold-up m^3/m^3
μ viscosity of the solution, kg/m s
ρ density, kg/m^3
σ surface tension of liquid, N/m
σ_c critical surface tension of packing material, N/m

Superscripts

g in gas phase
l in liquid phase

Subscripts

b in the bulk of the gas or liquid phase
i at gas–liquid interface

Acknowledgements

The support of this project by STW, the Dutch Technology Foundation and the support of the first author by Iranian Ministry of Since, Research and Technology are gratefully acknowledged.

References

Astarita, G., Savage, D. W., & Bisio, A. (1983). *Gas treating with chemical solvents*. New York: Wiley.

Brogren, C., & Karlsson, H. T. (1997). Modeling the absorption of SO_2 in a spray scrubber using the penetration theory. *Chemical Engineering & Technology*, *52*(18), 3085–3099.

Chang, C. S., & Rochelle, G. T. (1981). SO_2 absorption into aqueous solutions. *A.I.Ch.E. Journal*, *27*(2), 292–297.

Chang, C. S., & Rochelle, G. T. (1985). SO_2 absorption into NaOH and Na_2SO_3 aqueous solutions. *Industrial and Engineering Chemistry, Fundamental*, *24*(1), 7–11.

Danckwerts, P. V. (1970). *Gas–liquid reactions*. New York: McGraw-Hill.

Ebrahimi, S., Kleerebezem, R., van Loosdrecht, M. C. M., & Heijnen, J. J. (2003). Kinetics of the reactive absorption of hydrogen sulfide into aqueous ferric sulfate solutions. *Chemical Engineering Science*, *58*(2), 417–427.

Eden, D., & Luckas, M. (1998). A heat and mass transfer model for the simulation of the wet limestone flue gas scrubbing process. *Chemical Engineering & Technology*, *22*(1), 56–60.

Edward, T. J., Maurer, G., & Prausnitz, J. M. (1978). Vapour liquid equilibria in multicomponent aqueous solutions of volatile weak electrolytes. *A.I.Ch.E. Journal*, *24*(6), 966–975.

Gerard, P., Segantini, G., & Vanderschuren, J. (1996). Modeling of dilute sulfur dioxide absorption into calcium sulfite slurries. *Chemical Engineering Science*, *51*(12), 3349–3358.

Hikita, H., Asai, S., & Tsuji, T. (1977). Absorption of sulfur dioxide into aqueous sodium hydroxide and sodium sulfite solutions. *A.I.Ch.E. Journal*, *23*(4), 538–544.

Hikita, H., & Konishi, K. (1983). The absorption of SO_2 into aqueous Na_2CO_3 solutions accompanied by the desorption of CO_2. *Chemical Engineering Journal*, *27*(3), 167–176.

Karlsson, C. B. a. H. T. (1997). Modeling the absorption of SO_2 in a spray scrubber using the penetration theory. *Chemical Engineering Science*, *52*(18), 3085–3099.

Kenig, E. Y., Schneider, R., & Górak, A. (1999). Rigorous dynamic modelling of complex reactive absorption processes. *Chemical Engineering Science*, *54*(21), 5195–5203.

McCarthy, J. E. (1980). Flue gas desulfurization: Scrubber types and selection criteria. *Chemical Engineering Progress*, *76*(5), 58–62.

Onda, K., Sada, E., & Okumoto, Y. (1968a). Mass transfer coefficients between gas and liquid phases in packed columns. *Journal of Chemical Engineering of Japan*, *1*(1), 62–66.

Onda, K., Takahashi, M., & Okumoto, Y. (1968b). Mass transfer coefficients between gas and liquid phases in packed columns. *Journal of Chemical Engineering of Japan*, *1*(1), 56–62.

Parkhurst, D. L., & Appelo, C. A. J. (1999). *User's guide to PHREEQC (Version 2)*. U.S. Geological Survey, Denver, CO.

Reid, R. C., Prausnitz, J. M., & Poling, B. E. (1988). *The properties of gases and liquids*. New York: McGraw-Hill.

Sada, E., Kumazawa, H., & Butt, M. A. (1980). Absorption of sulfur dioxide into aqueous slurries of sparingly soluble fine particles. *Chemical Engineering Science*, *35*, 771–777.

Vanysek, P. (2001). *CRC handbook of chemistry and physics* (82nd ed.) (pp. 5–95 and 6–194). Boca Raton: CRC Press LLC.

Xia, J., Rumpf, B., & Maurer, G. (1999). Solubility of sulfur dioxide in aqueous solutions of acetic acid, sodium acetate, and ammonium acetate in the temperature range from 313 to 393 K at pressures up to 3.3 MPa: Experimental results and comparison with correlations/predictions. *Industrial & Engineering Chemistry Research*, *38*(3), 1149–1158.